THE JOURNAL OF BIOLOGICAL CHEMISTRY VOL. 285, NO. 23, pp. 18016–18024, June 4, 2010

Conserved Properties of Polypeptide Transport-associated (POTRA) Domains Derived from Cyanobacterial Omp85*[S]

Received for publication, February 9, 2010, and in revised form, March 22, 2010 Published, JBC Papers in Press, March 26, 2010, DOI 10.1074/jbc.M110.112649

Patrick Koenig[‡1], Oliver Mirus[§1], Raimund Haarmann[§], Maik S. Sommer[§], Irmgard Sinning[‡], Enrico Schleiff[§2], and Ivo Tews[‡3]

From the [‡]Heidelberg University Biochemistry Center (BZH), Im Neuenheimer Feld 328, 69120 Heidelberg and the [§]Department of Biosciences, JWGU Frankfurt am Main, Center of Membrane Proteomics and Cluster of Excellence Macromolecular Complexes, Max-von-Laue Strasse 9, 60439 Frankfurt, Germany

Proteins of the Omp85 family are conserved in all kingdoms of life. They mediate protein transport across or protein insertion into membranes and reside in the outer membranes of Gram-negative bacteria, mitochondria, and chloroplasts. Omp85 proteins contain a C-terminal transmembrane β-barrel and a soluble N terminus with a varying number of polypeptide-transport-associated or POTRA domains. Here we investigate Omp85 from the cyanobacterium *Anabaena sp.* PCC 7120. The crystallographic three-dimensional structure of the N-terminal region shows three POTRA domains, here named P1 to P3 from the N terminus. Molecular dynamics simulations revealed a hinge between P1 and P2 but in contrast show that P2 and P3 are fixed in orientation. The P2-P3 arrangement is identical as seen for the POTRA domains from proteobacterial FhaC, suggesting this orientation is a conserved feature. Furthermore, we define interfaces for protein-protein interaction in P1 and P2. P3 possesses an extended loop unique to cyanobacteria and *plantae*, which influences pore properties as shown by deletion. It now becomes clear how variations in structure of individual POTRA domains, as well as the different number of POTRA domains with both rigid and flexible connections make the N termini of Omp85 proteins versatile adaptors for a plentitude of functions.

Membrane proteins of the β-barrel type are pore proteins made up from a varying number of β-strands crossing the membrane. They are found exclusively in the outer membranes of bacteria, mitochondria, and chloroplasts (1). Specialized β-barrel proteins are involved in protein transport, called polypeptide-transporting β-barrel proteins (PTBs).[4] They can be divided into two classes according to their function (2–4). Class I PTBs are involved in transport of proteins from the periplasm to the extracellular space over the outer bacterial membrane. An example is the FhaC protein from *Bordetella pertussis*, belonging to the two-partner secretion system (4), which is required for transport of filamentous hemagglutinin. Class II proteins were initially discovered as surface-exposed antigens D15 and Oma87 from *Haemophilus influenza* (5, 6) and are now known to catalyze insertion of β-barrel proteins into the outer membrane (7–11). Analyzed members of this class include proteobacterial Omp85 proteins from *Neisseria meningitidis* (*e.g.* Refs. 12–14) and BamA from *Escherichia coli* (formerly named YaeT) (15–17), as well as Omp85 proteins from cyanobacteria like *Synechocystis* (18, 19) and *Anabaena* (20–22).

All PTBs share a common structure with a C-terminal β-barrel domain, forming a membrane pore and a soluble N-terminal region. The N terminus contains a varying number of so-called polypeptide transport-associated or POTRA domains: class I PTBs have two, class II PTB one to six POTRA domains (Table 1) (15, 23). The class I PTB FhaC from *B. pertussis* is known by crystallographic three-dimensional structure determination to comprise two POTRA domains and a 16-stranded β-barrel (24). For class II proteins, structural information is limited to the N-terminal POTRA domains. For *E. coli* BamA, five POTRA domains are seen in an extended conformation in solution in small angle x-ray scattering experiments (16). Two BamA crystal structures were reported both containing four of the five POTRA domains (15, 25). These structures are distinguished by a different conformation and thus reveal a hinge between the second and third POTRA domains.

A number of functions have been described for POTRA domains, namely to recognize target proteins directly or through binding of chaperones, or to play a structural role in formation of larger membrane protein complexes. A role in complex formation is known for the proteobacterial BamA and Omp85 proteins, which together with lipoproteins form a β-barrel assembly machinery (17, 26–29). Deletion of the BamA POTRA domains leads to dissociation of the β-barrel

* The work was supported by grants from the Deutsche Forschungsgemeinschaft (DFG SFB 807/P17 (to M. S. S., R. H., and E. S.) and SFB TR01/A10 (to O. M. and E. S.)), the Cluster of Excellence Frankfurt Macromolecular Complexes (to P. K. and E. S.), the Volkswagenstiftung (to E. S.), the interdisciplinary Ph.D. program "Molecular Machines: Mechanisms and Functional Interconnections" of the Land Baden-Württemberg (to P. K. and I. S.), and a collaborative research grant from the DFG (SFB 638 to I. S.).

[S] The on-line version of this article (available at http://www.jbc.org) contains supplemental "Experimental Procedures."

The atomic coordinates and structure factors (codes 3MC8 and 3MC9) have been deposited in the Protein Data Bank, Research Collaboratory for Structural Bioinformatics, Rutgers University, New Brunswick, NJ (http://www.rcsb.org/).

[1] Both authors contributed equally to this work.

[2] To whom correspondence may be addressed. E-mail: schleiff@bio.uni-frankfurt.de.

[3] To whom correspondence may be addressed. E-mail: ivo.tews@bzh.uni-heidelberg.de.

[4] The abbreviations used are: PTB, polypeptide-transporting β-barrel; MDS, molecular dynamics simulation; Omp85, outer membrane protein of 85 kDa; POTRA, polypeptide transport-associated domain; PDB, Protein data bank; MOPS, 4-morpholinepropanesulfonic acid.

TABLE 1

Analysis of the POTRA domain number in various organisms

Given are species, locus tag, bacterial class or organelle of occurrence, and the number of POTRA regions identified.

Species	Locus tag	Class/organelle	No. of POTRAs
N. meningitidis	Omp85	β-Proteobacteria	5
E. coli K12	BamA (YaeT)	γ-Proteobacteria	5
Campylobacter lari RM2100	D15	ϵ-Proteobacteria	5
Desulfovibrio desulfuricans	Oma87	δ-Proteobacteria	5
Rhodospirillum rubrum	Rrub1352	α-Proteobacteria	5
Chlorobium phaeobacteroides	D15	Green sulfur bacteria	5
Thermus thermophilus HB8	Omp	Deinococcus thermus	6
Fusobacterium nucleatum	FN1911	Fusobacteria	4
Anabaena sp. PCC 7120	Alr2269	Cyanobacteria	3
Arabidopsis thaliana	At5g19620	Plastid	3
A. thaliana	At3g46740	Plastid	3
A. thaliana	At5g05520	Mitochondria	1
Xenopus laevis	Oma87	Mitochondria	1

assembly machinery complex (15). In cyanobacteria like *Anabaena*, homo-oligomeric complexes exist *in vivo* (3), and oligomerization *in vitro* was found to be dependent on the POTRA region (20, 21). A receptor function is described for Omp85 from *Anabaena* (*ana*Omp85) determined by *in vitro* pulldown (21), and for POTRA domains of BamA, probed for by NMR spectroscopy (16). Recognition of periplasmic chaperones such as DsbA or SurA (30–32) is also required for proteobacterial membrane protein insertion. It was suggested that POTRA domains directly bind to these factors based on chemical cross-linking experiments (33).

Here, we report the structure of the *Anabaena* Omp85 POTRA domains, and derive common principles between proteobacterial and cyanobacterial POTRA domains. The similarities include interfaces on POTRA domains proposed in protein-protein interaction, and a hinge region between those domains. Differences must exist for pore gating as the long loop shown here to regulate pore activity is a unique structural feature seen in cyanobacteria and also predicted for *plantae*.

EXPERIMENTAL PROCEDURES

Molecular Biology—The construct used for protein expression includes amino acids 161–467 of wild-type *ana*Omp85-POTRA (alr2269) from *Anabaena sp.* PCC 7120 (21). Omitted are the predicted N-terminal signal sequence and the C-terminal pore-forming region. The construct has been cloned into a pET24a plasmid (Novagen, Madison, WI), using NdeI/XhoI restriction sites. Point mutations of *ana*Omp85-POTRA (F291M, L345M, and L373M) were generated using the QuikChange mutagenesis kit (Stratagene, La Jolla, CA).

Constructs *ana*Omp85 and *ana*Omp85-ΔN were previously described (21). *ana*Omp85-ΔL1 was generated from two fragments amplified by standard PCR on *alr2269* full-length cDNA: the coding region of Met^{1}–Phe^{387} was amplified using forward 5′-ATCGCCATGGAAGTGGCGGCTGTAGCAATCACA-3′ and 5′-TCCGCGGCCGCCAAAGCGGACGCTAATA-TTC-3′ reverse primers; the coding region of Arg^{403}–Phe^{833} was amplified using forward 5′-TTGGCGGCCGCGGACG-GACACAGGACTATATC-3′ and 5′-ATGCCTCGAGAAA-CCTTTCTCCAATACCG-3′ reverse primers. This introduces restriction sites NcoI/NotI and NotI/XhoI, respectively, required for cloning into pET21d. The sequence of the final construct was verified by automated sequencing.

Transport-specific Fractionation—E. coli BL21(DE3) star pRosetta cells were transformed with *ana*Omp85, *ana*Omp85-ΔL1, or *ana*Omp85-ΔN. Cells were incubated at 37 °C in 2YT medium and expression was induced by addition of 1 mM isopropyl 1-thio-β-D-galactopyranoside at A_{600} = 1. Cells were harvested 4 h after induction and resuspended in 50 mM Tris buffer at pH 8, containing 100 mM NaCl, 5 mM EDTA, 1 mM dithiothreitol, 0.5% (w/v) Triton X-100, and 5 mM β-mercaptoethanol. Cell lysis was performed on a French Press Cell Disruptor (Thermo Electron Corp., Germany) at 1200 p.s.i. Inclusion bodies were pelleted by centrifugation at 26,000 × *g* for 30 min at 4 °C. The pellet was washed with 20 mM Tris, pH 7.5, 200 mM NaCl, 10 mg/ml of deoxycholic acid, 10 mg/ml of Nonidet P-40, 10 mM β-mercaptoethanol, followed by two washes with 20 mM Tris, pH 7.5, 1 mM EDTA, 0.5% (w/v) Triton X-100, 5 mM β-mercaptoethanol, and one wash with 20 mM Tris, pH 8, 1 mM EDTA, 10 mM dithiothreitol. After each wash, the sample was centrifuged (17,000 × *g*, 4 °C, 10 min). The pellet was dissolved in 50 mM sodium phosphate buffer at pH 7, containing 8 M urea and 150 mM NaCl. For nickel-nitrilotriacetic acid chromatography (Qiagen, Hilden, Germany), the washing buffers used were first 50 mM Na-phosphate buffer, pH 7, containing 8 M urea, 150 mM NaCl, and 0.2% (v/v) Triton X-100, followed by 50 mM Na-phosphate buffer at pH 7, containing 8 M urea, 1 M NaCl, and 15 mM imidazole. The elution was performed with 50 mM Na-phosphate buffer, pH 7, containing 8 M urea, 150 mM NaCl, and 500 mM imidazole. Purified proteins were reconstituted into liposomes via dialysis with Mega-9 (*N*-nonanoyl-*N*-methylglucamine, Sigma) as previously described (20). The lipid, composed of L-α-phosphatidylcholine (type IV-S, Sigma) with 15 mol % of digalactosyl diglyceride (Nutfield Nurseries, UK) and 0.1 mol % of rhodamine-labeled phosphoethanolamine (Avanti Polar Lipids), was dissolved in 10 mM MOPS/Tris, pH 7, 80 mM Mega-9 to a concentration of 25.8 mM. Mega-9 was also added to the eluted proteins to a final concentration of 80 mM. Lipid and protein were thoroughly mixed in a ratio of 20:1 and incubated for 15 min at room temperature. The mixture was dialyzed against 10 mM MOPS/Tris, pH 7, at room temperature for 2 h, then at 4 °C overnight.

The modified protocol for transport-specific fractionation was previously described (21). In brief, two buffers containing 10 mM HEPES, pH 7.6, 0.1 mM EDTA, 0.1 mM EGTA, 10 mM KCl, and 459 mM urea (isosmotic to 400 mM sucrose (21)) were used to create isosmotic density gradients of 12 ml. These were layered with 200 μl of proteoliposomes each and centrifuged at 300,000 × *g* for 4 h at 4 °C. Derived fractions were examined via Western blot with antibody against *ana*Omp85 (21, 22).

Structure Determination—E. coli BL21(DE3) strains were transformed with *ana*Omp85-POTRA. Cells were grown in LB medium at 37 °C to an A_{600} of 0.6, and protein expression was then induced for 3 h by addition of 1 mM isopropyl 1-thio-β-D-galactopyranoside. Harvested cells were resuspended in 20 mM Tris-HCl buffer, pH 8.0, containing 200 mM NaCl and 10 mM imidazole, before lysis using an M110 microfluidizer at 15,000 p.s.i./100 megapascal (Microfluidics®). The soluble fraction of the lysate, cleared by ultracentrifugation, was loaded onto a HisTrap nickel affinity column (GE Healthcare), and eluted with buffer containing an additional 250 mM imidazole. The

TABLE 2
Crystallographic analysis

	*ana*Omp85		
	POTRA P1-P2-P3, "tetragonal," PDB 3MC8	POTRA F291M, selenomethionine, "SAD"[a]	POTRA P1-P2, "hexagonal," PDB 3MC9
Beamline, wavelength (Å)	ID29, 0.976	ID14-1, 0.933	ID23-1, 0.933
Space group	$P4_32_12$	$P4_32_12$	$P6_3$
Unit cell $a = b$, c (Å)	105.3, 83.3	105.5, 86.3	108.6, 60.4
Solvent content (%)	63	63	40
No. of molecules in AU[b]	1	1	2
Unique reflections	15,133	12,550	23,906
Mosaicity (°)	0.43	0.52	0.48
Average B (Å^2)	77.3	65.2	38.4
Resolution (Å)/HRS[c]	50-2.59/2.65-2.59	50-2.8/2.9-2.8	50-2.1/2.13-2.10
R_{sym} (%)[d]/HRS	9.9/47.2	10.4/70.6	10.2/49.8
Completeness (%)/HRS	100/100	100/100	100/100
⟨I⟩/⟨sigI⟩/HRS	26.4/6.9	23.2/2.75	14.7/3.2
Redundancy/HRS	20.3/18.7	28.1/28.1	7.8/7.7
Protein atoms, waters	2014, 34		2511, 153
Root mean square deviation bonds (Å), angles (°)	0.016/1.648		0.011/1.377
Ramachandran plot[e]	212/8/0/0		264/11/0/0
R_{free} (%)/R_{work} (%)[f]	28.08/22.63		24.5/19.54

[a] SAD, single-wavelength anomalous dispersion.
[b] AU, asymmetric unit.
[c] HRS, high resolution shell.
[d] $R_{sym} = \Sigma_h\Sigma_i||I(h)| - |I(h)_i||/\Sigma_h\Sigma_i|I(h)_i|$, where $I(h)$ is the mean intensity.
[e] Ramachandran plot values were determined by PROCHECK (40), the values are for residues in the favored/allowed/generously/disallowed regions.
[f] $R_{work} = \Sigma_h||F_{obs}(h)| - k|F_{calc}(h)||/\Sigma_h|F_{obs}(h)|$, where $F_{obs}(h)$ and $F_{calc}(h)$ are observed and calculated structure factors, respectively; 5% of the data were excluded to calculate R_{free}.

eluate was further purified by size exclusion chromatography on a S200 26/60 column (GE Healthcare), using 20 mM Tris-HCl buffer, pH 8.0, containing 200 mM NaCl. Purified protein was concentrated to about 0.65 mM prior to crystallization.

Crystallization was carried out in sitting-drop vapor diffusion experiments with a drop size of 1 μl at 20 °C. Crystals of the tetragonal space group appeared after 5 days from 0.1 M Tris buffer, pH 8.5, containing 0.8 M Na/K tartrate and 0.5% PEG-MME 5000. The hexagonal crystals appeared after approximately 2 months in 0.2 M calcium chloride and 20% PEG 3350. Crystals were flash-frozen in liquid nitrogen in crystallization buffer containing an additional 25% PEG 200 and stored.

All data were collected at the European Synchrotron Radiation Facility (ESRF, Grenoble, France), integrated, and scaled with the HKL software (34). Data reduction and free *R* assignment were carried out with the CCP4 suite of programs (35). Molecular replacement with structures of various POTRA domains was not successful (PDB codes 2qcz, 2qdf, 2vh1, 2vh2, and 2qdz). Heavy atom soaks for experimental phasing did not yield any suitable derivatives. Experimental phasing using methionines artificially introduced by site-directed mutagenesis and the selenomethionine phasing protocol are described under supplemental "Experimental Procedures." The structure of the hexagonal crystal form was determined by molecular replacement using the experimental tetragonal structure with the program Phaser (36). Iterative model building and refinement of both structures were carried out with the programs Coot (37) and REFMAC5 (38), cycled with ARP (39). The structure quality was accessed using PROCHECK (40). Coordinates as well as structure factors of native and SAD (single-wavelength anomalous dispersion) data have been deposited with the PDB under codes 3MC8 and 3MC9.

Molecular Dynamics Simulation—Molecular dynamics simulations were performed with GROMACS version 4 (41). MD simulations of four replicas as described under supplemental "Experimental Procedures" were set up with different random starting velocities with a targeted simulation time of 100 ns each. Swing and twist angles of POTRA domains as shown in Figs. 1 and 2 were calculated with a Yasara macro as described under supplemental "Experimental Procedures". All 400,000 structures from the trajectories of the MDSs were analyzed as well as all POTRA structures from the PDB.

Sequence Analysis—Sequences of PTBs were collected by multiple rounds of PSI-BLAST (NCBI website) (42). Sequences were aligned with MAFFT version 6.708b (43). Weblogo was used to generate the images presented (44).

RESULTS

Structure of the POTRA Region of Anabaena Omp85—A soluble fragment of the N-terminal periplasmic domain of *Anabaena sp.* PCC 7120 lacking the coding region for the N-terminal signal sequence (residues 161 to 470 (21)) and the C-terminal pore-forming β-barrel region was crystallized in two different crystal forms. Initial attempts to solve the structures by molecular replacement using either full-length, truncated or polyalanine models of known POTRA domains as search models failed (see "Experimental Procedures").

Due to the lack of methionines in the expression construct, hydrophobic residues in the core of the protein were exchanged with methionines by site-directed mutagenesis to allow for a selenomethionine phasing of the tetragonal crystal form (see supplemental "Experimental Procedures"). Molecular replacement was then used to determine the structure of the hexagonal crystal form. Data collection and refinement statistics are given in Table 2.

The tetragonal crystal form shows three POTRA domains in an extended arrangement, named P1 to P3 from the N terminus (Fig. 1*A*). The POTRA domains comprise residues 217 to 296 (P1), residues 297 to 377 (P2), and residues 378 to 467 (P3). The POTRA domains share a common fold of a three-stranded β-sheet packed against two helices (Fig. 1*A*, *inset*), with variation: P1 possesses a small two-stranded β-sheet near to its N

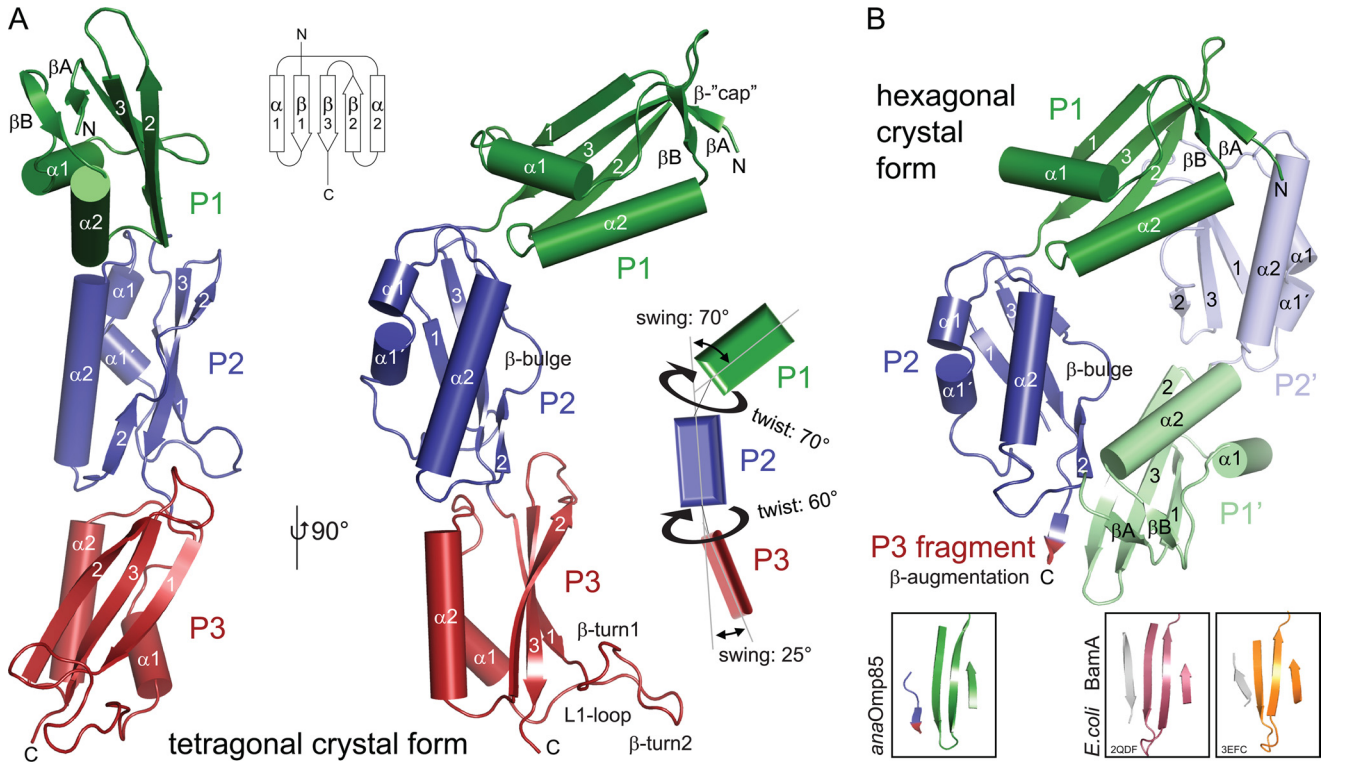

FIGURE 1. **Crystal structures of *ana*Omp85-POTRA.** *A*, the three POTRA domains, named P1, P2, and P3, are shown in *green*, *blue*, and *red*, respectively, as seen in the tetragonal crystal form. The two views are rotated by 90° around a vertical axis in the picture plane. Features discussed in the text, such as the β-cap, β-bulge, and L1-loop, are indicated. A secondary structure diagram is given for the common POTRA-fold (*top inset*). The schematic representation indicates the inclination of neighboring POTRA domains, here called swing angle, and the torsion of two POTRA domains about their principal axis, here called twist angle. *B*, in the hexagonal crystal form, *ana*Omp85-POTRA contains only POTRA domains P1 and P2, shown in *green* and *blue*, respectively. Two copies are seen in the asymmetric unit of the crystal, and β-augmentation is observed as indicated by the *red*/*blue* strand, representing parts of both, the P2 and P3 domains. This interaction mode is recurrent, and was also seen in the structures of *E. coli* BamA (15, 25), however, with variation with respect to the interaction and orientation of β-strands, see *insets*.

terminus, capping this domain; in P2, the helix α1 and the β-strand β1 are both interrupted; and in P3, an extended structured loop is seen between β1 and α2, forming two β-turns.

Observation of the hexagonal crystal form was fortuitous as a single crystal appeared after approximately 2 months. The expression construct and thus the protein used in crystallization was identical in both cases, however, crystals in the tetragonal space group typically appeared after a few days. In the hexagonal lattice only POTRA domains P1 and P2 were seen (Fig. 1*B*). Two P1-P2 fragments were found per asymmetric unit and form an antiparallel dimer. Part of the dimer contact is a small segment comprising the first six amino acids of P3, residues 378 to 384, which forms a β-strand that extends the β-sheet of P1. The hexagonal crystal packing does not allow space for the third POTRA domain, suggesting P3 may have degraded during the extended time of crystallization.

Dynamics of POTRA Domain Assembly—To understand whether the three POTRA domains are linked in a similar fashion to each other, we compared the relative positioning of the POTRA domains. For an analysis, a nomenclature is devised (see supplemental "Experimental Procedures"). Briefly, the central β-strand of each POTRA domain is chosen to define a major axis for each POTRA domain. Axes of neighboring domains define so called "swing" angles. Torsion around the axis, defined by taking the midpoint of α-helix α2 as reference, defines "twist" angles (Fig. 1*A*).

In the tetragonal crystal form (Fig. 1*A*) the P1 and P2 domains are rotated by a twist angle of about 70° relative to each other, and further tilted by a swing angle of 70°. The same arrangement is also seen in the hexagonal crystal form (Fig. 1*B*). This leads to a kink in the extended arrangement of the POTRA domains. The POTRA domains P2 and P3 are rotated by a twist angle of about 60° relative to each other. The swing angle is 25° smaller than seen for the P1-P2 conformation and leads to a more extended arrangement.

The now defined arrangement of POTRA domains in *ana*Omp85 was compared with POTRA structures in the protein data base (Fig. 2*A*). The orientation of P2-P3 (*open square*) matches the one observed for the two FhaC POTRA domains (*green square* (24)). The observed interfaces bury 470 Å^2 in *ana*Omp85 and 440 Å^2 in FhaC. Similar interactions contribute to the domain interface (Fig. 3) and involve: (*a*) a helix dipole formed by the α2-helices (compare Fig. 1*A*); (*b*) hydrogen bonds around a highly conserved glycine residue at the C terminus of α2; (*c*) a hydrophobic interaction where a valine side chain inserts in *trans* into a hydrophobic pocket of the N-terminal located POTRA domain; (*d*) hydrogen bonds formed with residues of the linker region between the two POTRA domains.

In contrast to the extended P2-P3 interaction, the interface of P1-P2 is smaller and buries only 260 Å^2. The conformation of P1-P2 (Fig. 2*A*, *open triangle*) is closest to the P2-P3 orientation

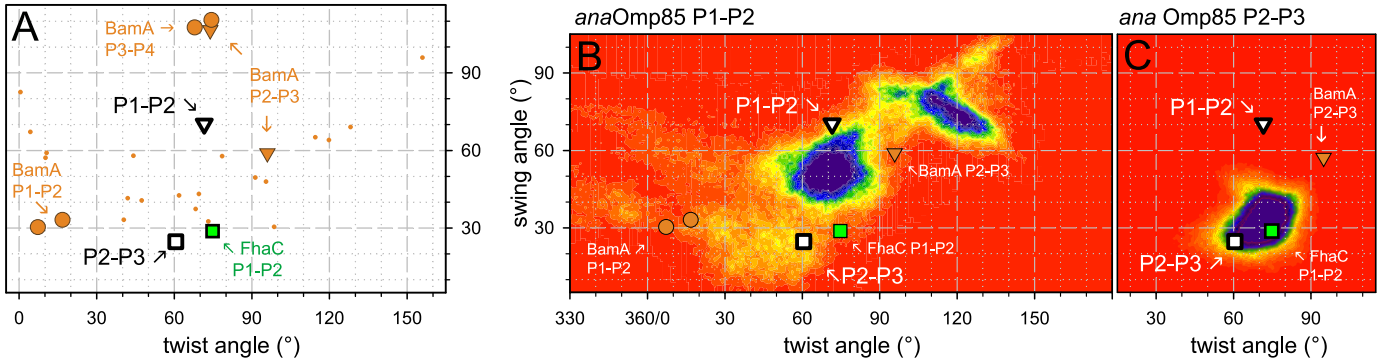

FIGURE 2. **Structural and molecular dynamics analyses.** *A*, twist and swing angles (as illustrated in Fig. 1) have been plotted for neighboring POTRA domains of various structures. Values for *ana*Omp85 are given as *open white symbols*: P1-P2, *open triangle*; P2-P3, *open square*. POTRA domains of the *E. coli* BamA (formerly known as YaeT) x-ray structures (PDB codes 2qdf and 3efc (15, 25)) are shown as *orange symbols*: for P1-P2, *circle*; for P2-P3, *triangle*; and P3-P4, *circle*. The *orange dots* represent the NMR ensemble of P1-P2 (PDB code 2v9h (16); *n.b.*, the flexibility observed in the NMR ensemble may be more restricted as suggested by a subsequent study on the same domains by PELDOR EPR spectroscopy (58)). The *green square* represents P1-P2 from FhaC (PDB code 2qdz (24)). *B* and *C*, based on simulations of 100 ns each in four replica, giving rise to 400,000 structures, twist and swing angles are plotted for P1 and P2 domains (*B*), as well as for P2 and P3 domains (*C*) (symbols as in *A*).

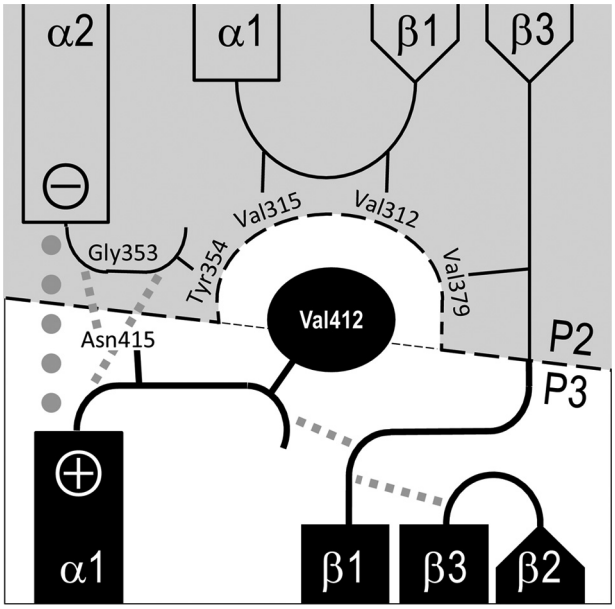

FIGURE 3. **Interface between P2 and P3.** The scheme shows selected secondary structure elements of P2 and P3, as labeled, loop regions and amino acid residues. Hydrogen bonds are indicated as *dashed lines* and occur mainly through backbone interactions. The *dotted line* indicates a possible helical dipole interaction.

from one (25) of two *E. coli* BamA crystal structures (15, 25) (*orange triangles*).

To assess the degree of freedom of angular motion of the *Anabaena* POTRA domains relative to each other, our method of choice was molecular dynamics simulation (MDS). The simulation boxes contained protein, water, and added counterions. The size of the simulation boxes was large enough to accommodate all theoretically possible angular conformations of the three POTRA domains. In total we performed four independent MDSs at 300 K of 100 ns each. The analysis shows a stable interaction for the P2-P3 domains (Fig. 2*C*) and flexibility in the P1-P2 interaction (Fig. 2*B*). For the latter, two dominant conformations are seen, and one is close to the one observed in the crystal (*open triangle*). The flexibility in the interaction between P1 and P2 is matching the observation of the smaller interface combined with a longer linker, compared with P2-P3, where a short connection and a larger interface are seen. The conformational freedom of the P2-P3 interaction is further restricted by loops between secondary structure elements that are longer in P2-P3 (in P2 between β1 and α1 and between α2 and β2; in P3 between β2 and β3) compared with P1-P2.

POTRA Domains Are Destined for Protein-Protein Interaction—POTRA domains are involved in formation of protein complexes, as introduced above. However, structures of complexes have not been determined so far and therefore, the structures of POTRA domains are analyzed for putative protein-protein interaction sites. In the *ana*Omp85 this analysis is supported by fortuitous observation of a crystal contact in the hexagonal crystal form: the β-sheet of P1 interacts through β2 with β-strands (Fig. 1*B*). This type of interaction in which a β-sheet and a β-strand or -sheet of an interaction partner associate is commonly known as β-augmentation (45), and has similarly been observed for BamA POTRA structures (15, 25). Aside from β-augmentation, in both our crystal forms there are structural features in P2 that deviate from the regular POTRA-fold (Fig. 4*A*). First, β-strand β2 is disrupted. This is equivalent to the observation in *E. coli* BamA POTRA domains where a β-bulge (46) is formed in the third POTRA domain.

The second structural feature seen in P2 is a short 3–10 helix insertion following helix α1. The side chain of Tyr^{329} located in this 3–10 helix points into a hydrophobic pocket sandwiched between helix α1 and the central β-sheet (Fig. 4*A*). Again, comparison with the *E. coli* POTRA structure shows that alternative conformations in this region exist in the third POTRA domain of BamA (15, 25) (Fig. 4*B*). MDS shows flexibility in this region. Notably, in all MDSs the Tyr^{329} side chain reversibly moves out of its pocket and in two out four MDSs strong backbone motion of the Tyr^{329} loop opens a hydrophobic pocket in a reversible manner (Fig. 4*C*). Consistently, Tyr^{329} is in a region with enhanced crystallographic *B*-factors indicative of increased mobility.

POTRA Domains and Pore Activity—The known class II PTB structures from the periplasmic domain of *E. coli* BamA do not contain the C-terminal POTRA domain adjacent to the pore. However, this particular POTRA domain is of special interest as

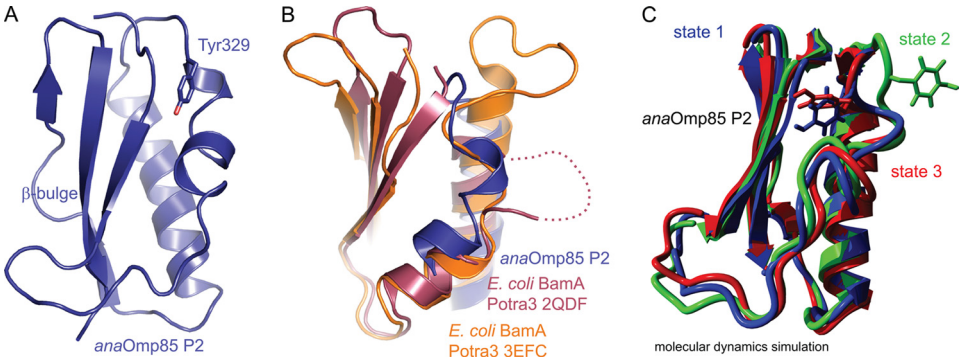

FIGURE 4. **Features of *ana*Omp85-P2.** *A*, the P2 domain contains two structural features that deviate from the regular structure (compare *inset* in Fig. 1*A*). The second β-strand β2 is interrupted to form a β-bulge structure. Likewise, the helix α1 is interrupted to form a shorter helix and a 3–10 helical segment; the side chain of Tyr^{329} folds back into a hydrophobic pocket (shown in stick representation). *B*, comparison of *ana*Omp85-P2 (*blue*) with the third POTRA domain of *E. coli* BamA shown in *red* and *orange* (PDB codes 2qdf and 3efc (15, 25)). The two *E. coli* structures reveal different conformations for the loop between α1 and α2. *C*, molecular dynamics simulation, showing three selected structures of P2 in which distinct positions of Tyr^{329} are observed. On the timeline of the MDS, the *blue* structure is followed by the *green* structure in which Tyr^{329} is displaced from the hydrophobic binding pocket, followed by the *red* structure in which Tyr^{329} is seen back in the hydrophobic binding pocket.

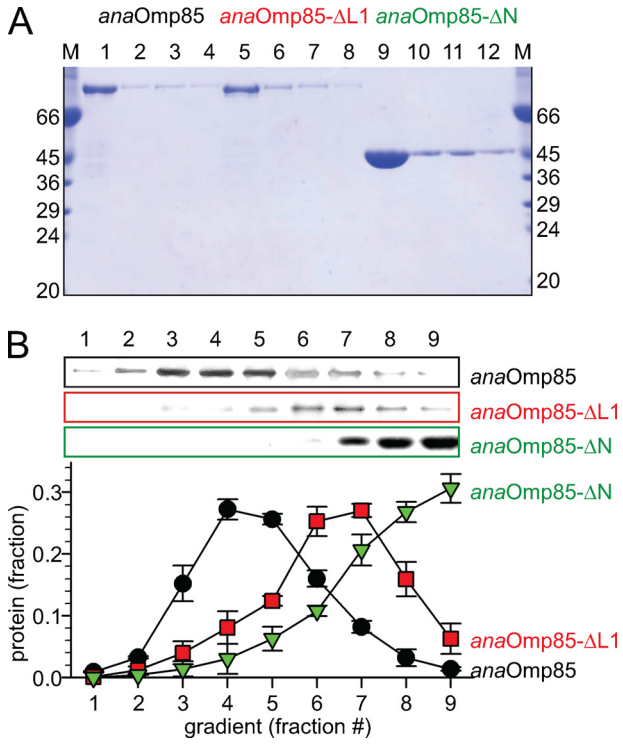

FIGURE 5. **Transport-specific fractionation of various Omp85 variants.** *A*, Coomassie stain SDS-PAGE of imidazole-eluted fractions after nickel affinity chromatography purification of *ana*Omp85 (*lanes 1–4*), *ana*Omp85-ΔL1 (*lanes 5–8*), and *ana*OMP85ΔN (*lanes 9–12*); the size of the molecular mass standard is given in kDa. *B*, proteoliposomes containing proteins as indicated and protein-free liposomes were separated on an isosmotic gradient. After centrifugation, fractions were analyzed by SDS-PAGE, followed by immunodecoration with antibodies against *ana*Omp85. The intensity of immunostaining was quantified and is presented as fraction of total protein in the graph.

it might be involved in regulation of the pore and thereby of protein transport. Indeed, deletion of this domain in Omp85 proteins leads to severe phenotypes in *E. coli* and *N. meningitidis* (15, 47, 48). This draws our attention to *ana*Omp85 P3 present in the structure derived from the tetragonal crystal form.

P3 has a unique 20-amino acid loop seen between β1 and α1 (Fig. 1*A*), which we termed "L1-loop." Pore properties of *ana*Omp85 were investigated regarding the influence of the POTRA domains and especially with respect to the L1-loop in a proteoliposome swelling assay. *ana*Omp variants were heterologously expressed, purified (Fig. 5*A*), and reconstituted into liposomes. The exchange of solutes is then determined by centrifugation, where penetration into the gradient indicates solvent exchange (21). Using this assay, we investigated Omp85 full-length protein (*ana*Omp85), protein truncated to the pore-forming region (*ana*Omp85-ΔN), and protein with a deletion of the L1-loop (*ana*Omp85-ΔL1). Proteoliposomes with full-length *ana*Omp85 (Fig. 5*B*, *circle*) show identical migration behavior with empty liposomes (as determined by rhodamine labeling, not shown), indicating that transport of osmolytes did not occur (compare Ref. 21). Hence, the full-length protein is tight against the solute exchange. In contrast, proteoliposomes with *ana*Omp85-ΔN (Fig. 5*B*, *triangle*) migrated into the gradient, consistent with transport activity. The L1-deletion variant *ana*Omp85-ΔL1 was investigated to estimate the contribution of the L1-loop in pore gating (Fig. 5*B*, *square*). Proteoliposomes with *ana*Omp85-ΔL1 show osmolyte transport at an intermediate level between proteoliposomes containing full-length *ana*Omp85 or the POTRA deletion variant *ana*Omp85-ΔN. The data demonstrate that the L1-loop has an influence on pore gating.

Conserved Structural Properties of the L1 Region—The L1-loop of *Anabaena* P3 forms two β-turns (Fig. 6). Alignment of cyanobacterial Omp85 proteins shows that the L1-loop region varies in length. Few L1-loops are predicted to be 5 or 31 amino acids in length, but most sequences fall into two distinct classes with lengths of 19/20 (long L1) or 12/13 amino acids (short L1) (compared in the table in Fig. 6). In *Nostocales*, to which *Anabaena* belongs, the 20-amino acid insertion is most common.

The secondary structure of a β-turn is four amino acids in length and (usually) requires a glycine at the fourth position (49). Sequence conservation suggests that two β-turns are common to long L1-loops; short L1-loops may still contain one β-turn (see sequence logos in Fig. 6). The L1-loop otherwise carries mostly charged amino acids like arginine, lysine, aspartate, and glutamate.

When the sequence analysis is extended to other class II PTBs, characteristic L1-loops are also seen in chloroplast Omp85 proteins of the Toc75 family (Toc75III (50) and Toc75V/Oep80 (51)), in mitochondrial proteins of the Sam50 family (52–54), and in proteobacterial proteins. All Omp85 proteins possess a conserved glycine, and thus all these proteins have the potential to form β-turn structures.

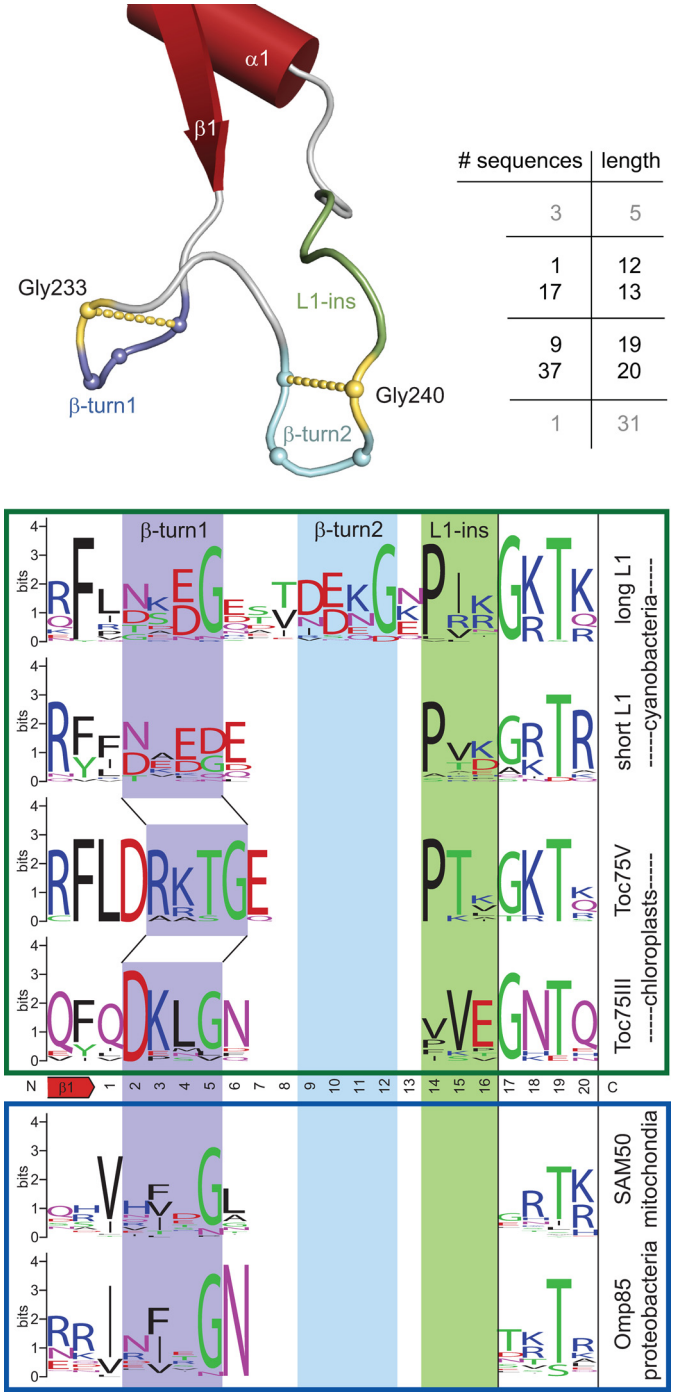

FIGURE 6. **The L1-loop of *ana*Omp85-P3.** The L1-loop from *Anabaena* Omp85, shown in schematic representation, is sited between β1 and α1 and is stabilized by two β-turn structures, involving conserved glycines. When cyanobacterial Omp85 proteins are compared, the length of the L1-loop is seen to vary (see table). Sequences are usually 19/20 (long L1-variant, as for *Anabaena*) or 12/13 residues in length (short L1 variant). The sequence logos are given for the long and short variant of cyanobacterial L1-regions, for chloroplast Toc75 proteins, for mitochondrial Sam50 proteins, and for proteobacterial Omp85 proteins. The *shaded* regions are shown in respective colors in the schematic.

A three-amino acid insertion seen in cyanobacterial L1-loops and Toc75 proteins unifies cyanobacteria and *plantae*, whereas mitochondrial and proteobacterial Omp85 proteins lack this motif. Interestingly, the insertion as well as the C-terminal L1-region and the N-terminal flanking sequences differ slightly in Toc75III proteins when compared with cyanobacterial Omp85 and Toc75V/Oep80 sequences, underpinning close relationship and divergence of Toc75III sequences (20). Proteobacterial and mitochondrial sequences are divergent from either motif. Class I proteins, in contrast, have L1-loops that are only 5 amino acids in length and are not known to form β-turns.

The long L1-loop, conserved in sequence and structure, is identified as a regulatory element in cyanobacterial Omp85 pore gating (Fig. 5). The specific L1-loop sequence marks unique properties between class II PTB families (Fig. 6), the meaning of which remains to be explored.

DISCUSSION

Omp85 proteins are essential constituents of the outer membranes of Gram-negative bacteria, eukaryotic mitochondria, and chloroplasts (7–9, 11). We studied the cyanobacterial class II polypeptide-transporting β-barrel protein Omp85 (21, 22). The protein has a predicted 16-stranded β-barrel pore at the C terminus and contains a periplasmic region, which is shown here by three-dimensional structural analysis to possess three POTRA domains (Fig. 1*A*).

The periplasmic regions are known to be regulators of pore function in class I and class II PTBs (20, 24), although the precise mechanism of gating remained elusive. Previously, two crystallographic structures of the POTRA region of the class II PTB BamA from *E. coli* were reported; however, neither resolved the C-terminal POTRA domain (15, 25). Two important insights are gained from knowledge of the three-dimensional structure of this domain. First, it contains the extended L1-loop between strand β1 and helix α1. The L1-loop takes part in gating, as seen from the transport-specific fractionation of proteoliposomes (Fig. 5*B*). Second, the domain is seen in fixed arrangement with the POTRA domain preceding it (Fig. 2*C*), suggesting these POTRA domains form a functional unit.

Analysis of class I and class II PTBs demonstrated that a fixed arrangement is conserved for the two most C-terminal domains (Fig. 2*C*), as seen in the full-length structure of the class I PTB FhaC (24). This now allows superposing P2-P3 with the two POTRA domains of FhaC (Fig. 7). In doing the L1-loop points away from the pore, and could interact with the membrane, or alternatively with additional proteins. The L1-loop contains conserved β-turns (Fig. 6), and these secondary structures are documented protein-protein interaction motifs (49). However, the POTRA domains in FhaC are involved in crystal packing, and the superposition may thus not reflect the state in solution, if the POTRA domains are able to rotate.

Besides pore gating, the periplasmic region of Omp85 serves as an interaction surface. Protein-protein interactions are required for the assembly of larger protein complexes (17, 29), for homo-oligomerization (14, 21), binding of protein transport-associated factors, such as chaperones (33) or β-barrel substrate proteins (16, 17). A number of features are identified in the *Anabaena* POTRA structures highlighting potential protein-protein interfaces. One mode by which POTRA domains interact with other proteins may be β-augmentation, an interaction that involves complementation of a β-sheet with a β-strand of a second protein. This is largely sequence-unspecific because it involves contacts through

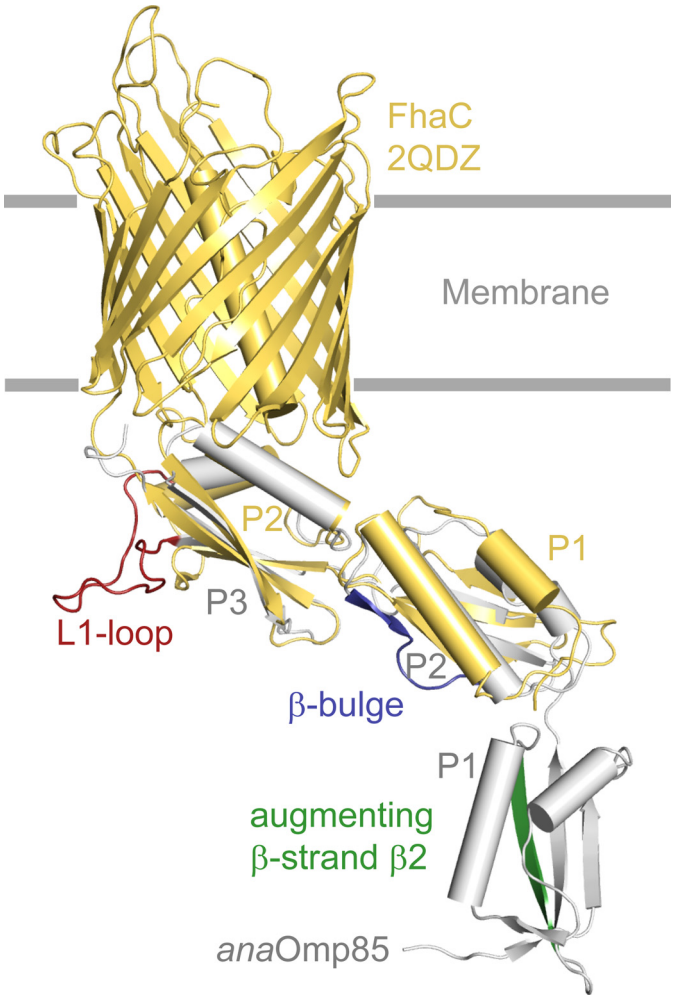

FIGURE 7. **Structural superposition of POTRA domains P2 and P3 of *ana*Omp85 with POTRA domains P1 and P2 from FhaC (*gold*, PDB code 2QDZ (24)).** *ana*Omp85 is shown in *gray*, highlighted are the structural features discussed: β-strand β2 of P1, *green*; and the β-bulge structure inserted into β2 of P2, *blue*, both implied in the protein interaction; and the L1-loop in P3, *red*.

backbone atoms (55). We observe β-augmentation in the hexagonal crystal form, namely between P1 and a β-strand from P3 (Fig. 1*B*). A similar observation was made for BamA, where β-augmentation occurs between the third POTRA domain and a β-strand that is a remnant of the fifth POTRA domain (15, 25). Interestingly, the exact mode by which β-augmentation takes place differs. Kim *et al.* (15) and ourselves (Fig. 1*B*) observed a parallel alignment of the augmenting β-strand with the adjoining β-sheet; Gatzeva-Topalova *et al.* (25) observed an antiparallel mode. Directionality would thus have to be provided by interactions outside of this region. Short peptides derived from the *E. coli* OMP PhoE have been shown by NMR titration to interact weakly with the edges of the β-sheet of P1 and P2 of *E. coli* BamA (16) supporting the notion of β-augmentation as a general motif for protein recognition by POTRA domains.

Further protein interfaces are predicted on either side of the β-sheet of *ana*Omp85 P2 (Fig. 4), which are similar to those seen in the third POTRA domain of BamA. In both POTRAs the second β-strand is disrupted through formation of a β-bulge structure (Fig. 4, *A* and *B*). This feature is important as amino acid replacements in this region change specificity with respect to complex formation (15). In addition, helix α2 in P2 is also interrupted to form a regular helix and a smaller 3–10 helical segment (Fig. 1*A*). Two conformations are seen in this region in MDS, as a flipping of a tyrosine residue opens a hydrophobic pocket in P2 (Fig. 4*C*). This may be important when considering that β-barrel proteins that are substrates to Omp85 share a conserved C-terminal phenylalanine (56). Although we were unable to demonstrate an interaction with hydrophobic amino acids or peptide substrates experimentally, flexibility in this region gives evidence for existence of an additional interface for protein-protein interaction. Support comes from structure comparison with *E. coli* BamA where two different conformations in this region have been observed for the third POTRA domain in the two crystal structures determined (15, 25).

Provisional functions can now be assigned to the three POTRA domains of *ana*Omp85: P3 is implied in regulation of protein transport through its L1-loop, which is consistent with the importance of the POTRA domain preceding the pore domain (14, 15, 21, 47, 48). Domains N-terminal might have functions in substrate recognition and hetero-oligomerization. Indeed, P1 is shown to have the propensity for protein-protein interaction by β-augmentation (Fig. 1*B*) and P2 has two potential protein interfaces to the sides of its β-sheet (Fig. 3). The flexibility between P1 and P2 domains (Fig. 2*B*) corresponds to flexibility of the second and third POTRA domains of *E. coli* BamA, observed in two crystal structures (15, 25), suggesting an equivalence of a hinge region. Protein-protein interaction might cause the relative orientation of P1 toward P2 to change. This is consistent with the proposal that two POTRA domains are required for substrate recognition (16). Therefore a hallmark of substrate-recognizing POTRA domains may be the flexible linker between them.

A final question concerns the varying number of POTRA domains in class II PTBs (Table 1) (23). Gatzeva-Topalova and co-workers (25) argued that larger POTRA structures may be required for bridging the periplasm, suggesting why five POTRA domains are identified in proteobacteria, and six in the genera *Deinococcus* and *Thermus*. Alternatively, the differences in POTRA number might be caused by different protein-protein interactions, because the periplasmic space of cyanobacteria can be even larger than that of proteobacteria, and cyanobacterial Omp85 proteins have less than 5 POTRA domains. The number of POTRA domains would then be an adaptation to different sets of accessory proteins.

Eukaryotic POTRA-containing sequences may have lost (several) POTRA domains with respect to the "ancestral" clades, due to altered functional requirements. Mitochondrial Sam50 has only one POTRA domain, and chloroplastidal Toc75-like PTBs typically have three POTRA domains, just as cyanobacteria (Table 1). Toc75 proteins are adapted to protein translocation across the membrane rather than the insertion into the membrane. The POTRA domains might be involved in protein recognition and transport, or in the adaptation to the

new interaction partners like the Toc or Tic components, dependent on the orientation of the protein within the membrane, which is unknown at present. The mode of substrate perception and thus POTRA domain number may differ through a different set of associated factors.

Further structure determinations of POTRA structures and more detailed functional studies establishing the accessory components and their role in OMP biogenesis are required to fully understand the diverse nature of POTRA regions. Despite existing differences between Omp85 proteins, as *e.g.* demonstrated by the inability of *ana*Omp85 to complement a *bamA* mutant (57), we demonstrate here that the functional elements are conserved among bacterial PTBs of class II. We will in the future address the properties of the defined units and in particular the function of the L1-loop.

Acknowledgments—Special thanks to Elmar Krieger for providing a Yasara macro for POTRA twist/swing angle calculations. We thank Jürgen Kopp and Claudia Siegmann from the Crystallization Platform (BZH/Cluster of Excellence: CellNetworks) for carrying out the automated crystallization screens and the European Synchrotron Radiation Facility for access to beamlines and for excellent user support. Goran Stjepanovic kindly carried out mass spectrometry analysis of selenomethionine-labeled proteins.

REFERENCES

1. Schulz, G. E. (2000) *Curr. Opin. Struct. Biol.* **10,** 443–447
2. Inoue, K., and Potter, D. (2004) *Plant J.* **39,** 354–365
3. Moslavac, S., Mirus, O., Bredemeier, R., Soll, J., von Haeseler, A., and Schleiff, E. (2005) *FEBS J.* **272,** 1367–1378
4. Jacob-Dubuisson, F., Villeret, V., Clantin, B., Delattre, A. S., and Saint, N. (2009) *Biol. Chem.* **390,** 675–684
5. Ruffolo, C. G., and Adler, B. (1996) *Infect. Immun.* **64,** 3161–3167
6. Thomas, W. R., and Rossi, A. A. (1986) *Infect. Immun.* **52,** 812–817
7. Bos, M. P., and Tommassen, J. (2004) *Curr. Opin. Microbiol.* **7,** 610–616
8. Gentle, I. E., Burri, L., and Lithgow, T. (2005) *Mol. Microbiol.* **58,** 1216–1225
9. Knowles, T. J., Scott-Tucker, A., Overduin, M., and Henderson, I. R. (2009) *Nat. Rev. Microbiol.* **7,** 206–214
10. Ruiz, N., Kahne, D., and Silhavy, T. J. (2006) *Nat. Rev. Microbiol.* **4,** 57–66
11. Schleiff, E., and Soll, J. (2005) *EMBO Rep.* **6,** 1023–1027
12. Bos, M. P., Robert, V., and Tommassen, J. (2007) *EMBO Rep.* **8,** 1149–1154
13. Manning, D. S., Reschke, D. K., and Judd, R. C. (1998) *Microb. Pathog.* **25,** 11–21
14. Robert, V., Volokhina, E. B., Senf, F., Bos, M. P., Van Gelder, P., and Tommassen, J. (2006) *PLoS Biol.* **4,** e377
15. Kim, S., Malinverni, J. C., Sliz, P., Silhavy, T. J., Harrison, S. C., and Kahne, D. (2007) *Science* **317,** 961–964
16. Knowles, T. J., Jeeves, M., Bobat, S., Dancea, F., McClelland, D., Palmer, T., Overduin, M., and Henderson, I. R. (2008) *Mol. Microbiol.* **68,** 1216–1227
17. Wu, T., Malinverni, J., Ruiz, N., Kim, S., Silhavy, T. J., and Kahne, D. (2005) *Cell* **121,** 235–245
18. Reumann, S., Davila-Aponte, J., and Keegstra, K. (1999) *Proc. Natl. Acad. Sci. U.S.A.* **96,** 784–789
19. Bölter, B., Soll, J., Schulz, A., Hinnah, S., and Wagner, R. (1998) *Proc. Natl. Acad. Sci. U.S.A.* **95,** 15831–15836
20. Bredemeier, R., Schlegel, T., Ertel, F., Vojta, A., Borissenko, L., Bohnsack, M. T., Groll, M., von Haeseler, A., and Schleiff, E. (2007) *J. Biol. Chem.* **282,** 1882–1890
21. Ertel, F., Mirus, O., Bredemeier, R., Moslavac, S., Becker, T., and Schleiff, E. (2005) *J. Biol. Chem.* **280,** 28281–28289
22. Nicolaisen, K., Mariscal, V., Bredemeier, R., Pernil, R., Moslavac, S., López-Igual, R., Maldener, I., Herrero, A., Schleiff, E., and Flores, E. (2009) *Mol. Microbiol.* **74,** 58–70
23. Sánchez-Pulido, L., Devos, D., Genevrois, S., Vicente, M., and Valencia, A. (2003) *Trends Biochem. Sci.* **28,** 523–526
24. Clantin, B., Delattre, A. S., Rucktooa, P., Saint, N., Méli, A. C., Locht, C., Jacob-Dubuisson, F., and Villeret, V. (2007) *Science* **317,** 957–961
25. Gatzeva-Topalova, P. Z., Walton, T. A., and Sousa, M. C. (2008) *Structure* **16,** 1873–1881
26. Charlson, E. S., Werner, J. N., and Misra, R. (2006) *J. Bacteriol.* **188,** 7186–7194
27. Malinverni, J. C., Werner, J., Kim, S., Sklar, J. G., Kahne, D., Misra, R., and Silhavy, T. J. (2006) *Mol. Microbiol.* **61,** 151–164
28. Sklar, J. G., Wu, T., Gronenberg, L. S., Malinverni, J. C., Kahne, D., and Silhavy, T. J. (2007) *Proc. Natl. Acad. Sci. U.S.A.* **104,** 6400–6405
29. Volokhina, E. B., Beckers, F., Tommassen, J., and Bos, M. P. (2009) *J. Bacteriol.* **191,** 7074–7085
30. Eppens, E. F., Nouwen, N., and Tommassen, J. (1997) *EMBO J.* **16,** 4295–4301
31. Lazar, S. W., and Kolter, R. (1996) *J. Bacteriol.* **178,** 1770–1773
32. Rouvière, P. E., and Gross, C. A. (1996) *Genes Dev.* **10,** 3170–3182
33. Sklar, J. G., Wu, T., Kahne, D., and Silhavy, T. J. (2007) *Genes Dev.* **21,** 2473–2484
34. Otwinowski, Z., and Minor, W. (1997) *Methods Enzymol.* **276,** 307–326
35. Collaborative Computational Project Number 4 (1994) *Acta Crystallogr. Sect.* D **50,** 760–763
36. McCoy, A. J., Grosse-Kunstleve, R. W., Adams, P. D., Winn, M. D., Storoni, L. C., and Read, R. J. (2007) *J. Appl. Crystallogr.* **40,** 658–674
37. Emsley, P., and Cowtan, K. (2004) *Acta Crystallogr. Sect.* D **60,** 2126–2132
38. Murshudov, G. N., Vagin, A. A., and Dodson, E. J. (1997) *Acta Crystallogr.* **53,** 240–255
39. Lamzin, V. S., and Wilson, K. S. (1997) *Methods Enzymol.* **276,** 269–305
40. Laskowski, R. A., MacArthur, M. W., Moss, D. S., and Thornton, J. M. (1993) *J. Appl. Cryst.* **26,** 283–291
41. Hess, B., Kutzner, K., van der Spoel, D., and Lindahl, E. (2008) *J. Chem. Theory Comput.* **4,** 435–447
42. Mirus, O., Strauss, S., Nicolaisen, K., von Haeseler, A., and Schleiff, E. (2009) *BMC Biol.* **7,** 68
43. Katoh, K., and Toh, H. (2008) *Brief Bioinform.* **9,** 286–298
44. Crooks, G. E., Hon, G., Chandonia, J. M., and Brenner, S. E. (2004) *Genome Res.* **14,** 1188–1190
45. Harrison, S. C. (1996) *Cell* **86,** 341–343
46. Richardson, J. S., Getzoff, E. D., and Richardson, D. C. (1978) *Proc. Natl. Acad. Sci. U.S.A.* **75,** 2574–2578
47. Amadasi, A., Bertoldi, M., Contestabile, R., Bettati, S., Cellini, B., di Salvo, M. L., Borri-Voltattorni, C., Bossa, F., and Mozzarelli, A. (2007) *Curr. Med. Chem.* **14,** 1291–1324
48. Méli, A. C., Hodak, H., Clantin, B., Locht, C., Molle, G., Jacob-Dubuisson, F., and Saint, N. (2006) *J. Biol. Chem.* **281,** 158–166
49. Koch, O., and Klebe, G. (2009) *Proteins* **74,** 353–367
50. Baldwin, A., Wardle, A., Patel, R., Dudley, P., Park, S. K., Twell, D., Inoue, K., and Jarvis, P. (2005) *Plant Physiol.* **138,** 715–733
51. Eckart, K., Eichacker, L., Sohrt, K., Schleiff, E., Heins, L., and Soll, J. (2002) *EMBO Rep.* **3,** 557–562
52. Gentle, I., Gabriel, K., Beech, P., Waller, R., and Lithgow, T. (2004) *J. Cell Biol.* **164,** 19–24
53. Kozjak, V., Wiedemann, N., Milenkovic, D., Lohaus, C., Meyer, H. E., Guiard, B., Meisinger, C., and Pfanner, N. (2003) *J. Biol. Chem.* **278,** 48520–48523
54. Paschen, S. A., Waizenegger, T., Stan, T., Preuss, M., Cyrklaff, M., Hell, K., Rapaport, D., and Neupert, W. (2003) *Nature* **426,** 862–866
55. Remaut, H., and Waksman, G. (2006) *Trends Biochem. Sci.* **31,** 436–444
56. Struyvé, M., Moons, M., and Tommassen, J. (1991) *J. Mol. Biol.* **218,** 141–148
57. Wunder, T., Bredemeier, R., Ruprecht, M., and Schleiff, E. (2009) *Endocytobiosis Cell Res.* **19,** 20–30
58. Ward, R., Zoltner, M., Beer, L., El Mkami, H., Henderson, I. R., Palmer, T., and Norman, D. G. (2009) *Structure* **17,** 1187–1194